ACS OMEGA

Open Access

http://pubs.acs.org/journal/acsodf

Article

Rhamnolipid-Modified PHB−Ectoine Nanoparticles for Multifunctional Skin Protection Against UVB, Irritation, and Bacteria

Alma Tyara Simbara, Fera Faridatul Habibah, and Rukman Hertadi*

Cite This: *ACS Omega* 2025, 10, 12200−12213

Read Online

ACCESS | Metrics & More | Article Recommendations | Supporting Information

ABSTRACT: Rhamnolipid, poly(*R*)-3-hydroxybutyrate (PHB), and ectoine are sustainable compounds produced by specific bacteria known for their protective benefits, including promoting skin health in applications, such as facial wash, sunscreens, and moisturizers. These compounds have been extensively studied due to their unique physicochemical properties and biocompatibility. Leveraging these beneficial properties, this study aimed to create a multifunctional protective formulation by synthesizing nanoparticles from PHB and ectoine, which are acknowledged for their anti-ultraviolet B (UVB) and anti-irritation properties. The covalent bonding of PHB and ectoine was achieved using 1-ethyl-3-(3-dimethylaminopropyl)carbodiimide (EDC), and the nanoparticles were produced through centrifugation. The synthesized nanoparticle (PHB−ectoine NPs) was physicochemically characterized and tested for anti-irritation and anti-UVB properties in vitro. The characterization revealed a homogeneous spherical shape with a distinct layered structure, primarily composed of carbon and oxygen. The PHB−ectoine NPs measured 527 ± 228 nm in size, had a zeta potential of −61.47 ± 0.64 mV, and exhibited notably higher anti-irritant and anti-UVB activities compared to PHB alone, by over 10 and 4 times, respectively. Furthermore, the addition of a rhamnolipid solution as a dispersant provided the nanofluid with antibacterial properties against *Staphylococcus aureus*. These results indicate that the rhamnolipid−PHB−ectoine nanoformulation shows significant potential as a multifunctional skin protective agent with anti-irritation, anti-UVB, and antibacterial capabilities.

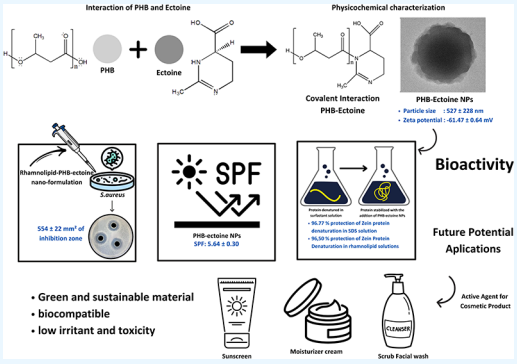

1. INTRODUCTION

Skin is the largest human organ, accounting for 16% of total body weight, and it covers the outside of the body.[1] Skin functions as a mechanical barrier, an immune system, and a sensor to regulate body temperature or synthesize vitamin D.[2−5] The integrity of the skin is compromised by internal and external factors, such as protein deficiency, vitamin shortage, radiation, chemicals, and microorganisms. These factors affect the structure and function of the skin, which increases the susceptibility to dermatological disorders or skin diseases.[6]

Cosmetics have been used for centuries to preserve the cleanliness, beauty, health, and integrity of the skin.[7] In general, cosmetics consist of a combination of water, emulsifiers, thickeners, fragrances, pH stabilizers, preservatives, and cosmeceuticals.[8] Many of these materials are derivatives of petroleum or mineral oil, which are not biodegradable and are dangerous to the skin.[9] In 2019, Panico et al. reported several dangerous compounds contained in 283 cosmetic products on the market. Benzophenone, toluene, dibutyl phthalate, limonene, parabens, and heavy metals, which are often used as sunscreens, cosmetic solvents, fragrances, preservatives, and whitening agents, are allergens, irritants, carcinogens, and toxicants for humans.[10] To address these concerns, much research has focused on sustainable and natural cosmetics derived from microbes and enzymes, such as PHB, ectoine, and rhamnolipid.[11−14]

PHB is a natural biopolymer belonging to the short-chain-length polyhydroxyalkanoates (scl-PHAs) family, characterized by 3−5 carbon chains.[15] It is synthesized by various bacteria, such as *Cupriavidus necator*, as intracellular granules under nutrient-limiting conditions with an excess of carbon source.[16,17] PHB is highly biocompatible, biodegradable, and nontoxic, making it an excellent candidate for applications in bioplastics, medical devices, and cosmetics.[18−21] To broaden its applications, PHB has been tailored by modifying its properties.[22] In 2018, Lin et al. prepared antibacterial hydrophobic nanofibrous membranes by electrospinning PHB and poly(butyleneadipate-*co*-terephthalate) (PBAT) grafted with 1-allylhydantoin and perfluorooctyl acrylate. The results showed that the membrane exhibited significant bacterial reduction, good hydrophobicity, and UV-A stability.[23]

Received: November 21, 2024
Revised: February 14, 2025
Accepted: February 20, 2025
Published: March 17, 2025

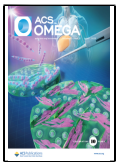

In the cosmetic field, PHB has been reported to be nontoxic to skin keratinocytes, making it suitable for topical use on the skin.[24] Prior studies have observed that PHB could stabilize a drug delivery system of liposomes, control the release of active agents in the skin, while increasing the UV light scattering effect by doubling the sun protection factor (SPF) value.[25] Other literature studies also show that PHB can be used as an exfoliating agent in cosmetic products. Beyond its biocompatibility and mechanical properties, PHB also exhibits piezoelectric behavior, with a piezoelectric constant comparable to collagen (d_{14} = 1.6−2.0 pC/N). This property allows PHB to generate surface polarization under mechanical deformation, which may influence its biological interactions, including antibacterial activity and skin protection. Previous studies have demonstrated that piezoelectricity in biomaterials can modulate bacterial adhesion and cellular responses, suggesting a potential role in enhancing PHB's efficacy in cosmetic applications.[26] In addition, the presence of an electric field at the material's surface has been linked to increased antimicrobial properties through electrostatic interactions and reactive oxygen species (ROS) generation.[27] While the direct influence of PHB's piezoelectricity on skin protection has not been fully explored, these findings open new avenues for understanding its multifunctionality in cosmetic formulations. Moreover, in 2025, Choi and Choi produced indirubin-incorporated PHB microbeads with potential for facial cleansers and eco-friendly future cosmetics.[28] While PHB has nontoxic, SPF, and exfoliation properties to be used in cosmetic products, other materials such as moisturizers are usually added to the cosmetic formulations to avoid irritation on the skin.[29]

Ectoine (2-methyl-1,4,5,6-tetrahydropyrimidine-4-carboxylic acid) is one of the cosmeceuticals produced by halophilic bacteria, with a structure that can promote hydrogen bonding in aqueous solutions.[30] Ectoine can bind water and form an ectoine-hydro complex that acts as a protective layer on the surface of cells and macromolecules. This allows ectoine to stabilize cell membranes, proteins, nucleic acids, complexes of DNA-proteins, and skin tissue.[31] The characteristics of ectoine have been explained by molecular dynamic simulations that show the cluster of water around ectoine is stable for a long period of time.[32] Ectoine can bind strongly to water and prevent the loss of transepidermal water, which is beneficial for moisturizers and acts as an anti-irritant in cosmetic formulations.[33]

Another material used in cosmetic formulations is a surfactant. Surfactants have functions such as foaming, emulsifying, and wetting agents.[34−36] However, synthetic surfactants are non-biodegradable and become toxic to humans and the environment.[37] As concerns in the cosmetic field, synthetic surfactants are reported to be more aggressive toward the skin and capable of causing irritation and allergic reactions.[38,39] In comparison, surfactants produced by microorganisms (biosurfactants) are less irritant with low skin toxicity, excellent surface properties, and stability at extreme pH, temperature, and salinity. This makes biosurfactants an alternative to synthetic surfactants in cosmetic formulations.[40] One biosurfactant currently attracting the attention of researchers is rhamnolipid.[41]

Rhamnolipid is a biosurfactant belonging to the glycolipid group, composed of a rhamnose sugar moiety and β-hydroxy fatty acid chains, typically C10−C14.[42] The primary producer of rhamnolipid is*Pseudomonas aeruginosa*.[43] Unlike medium-chain-length polyhydroxyalkanoates (mcl-PHA), which are intracellular polymers accumulated as granules for energy storage under nutrient-limiting conditions with excess carbon, rhamnolipids are extracellular biosurfactants synthesized to reduce surface tension and facilitate the emulsification of hydrophobic substances under nitrogen-limiting conditions combined with excess carbon sources.[44,45] The unique amphiphilic structure of rhamnolipids gives them exceptional surfactant and chelating properties. Furthermore, rhamnolipid exhibits favorable characteristics, including low toxicity, high biocompatibility, biodegradability, and excellent bioavailability.[46] These properties make rhamnolipids valuable in various applications, particularly in the health sector, where they have demonstrated anticancer, antifungal, antiviral, and antibacterial activities.[47,48] In addition, their significant emulsifying activity makes them a promising alternative to synthetic surfactants in cosmetic formulations, serving as emulsifiers, foaming agents, and active antibacterial agents.[49]

Other studies using nanotechnology in the field of cosmetics reveal an increase in the activity of the active ingredients found in cosmetics. It has been stated that nanoparticles with a size range from 10 to 1000 nm can easily be absorbed into skin pores and improve their efficacy.[50] In 2024, Phothong et al. used PHB to encapsulate astaxanthin as an exfoliator that does not cause sensitization or irritation to the skin. The research results showed that PHB-based active compounds are not toxic according to ISO 10993-5 and have the potential to be used in cosmetics.[21] In this study, a new material will be prepared based on the combination of PHB and ectoine to form nanoparticles (PHB−ectoine NPs) by using the cross-linking method with additions of 1-ethyl-3-(3-dimethylaminopropyl) carbodiimide (EDC). The prepared PHB−ectoine NPs were characterized by FTIR, NMR, SEM-EDX, TEM, PSA, and zeta potential. Furthermore, rhamnolipids will be used as antibacterial and dispersant agents of PHB−ectoine NPs in the formulations. Regarding their application in the cosmetic field, the resulting material is tested for its anti-irritant, anti-UVB, and antibacterial activities. Their antibacterial activity will be tested against Gram-positive bacteria*Staphylococcus aureus* (*S. aureus*) and Gram-negative bacteria*Escherichia coli* (*E. coli*) using well diffusion methods. Meanwhile, the anti-irritant activities are gravimetrically analyzed using the Zein protein method, and the anti-UVB value is obtained from the ultraviolet spectrophotometry method.

The versatility of PHB as a natural polyester that can undergo chemical modification has been emphasized in various studies. Lenz and Marchessault (2005) highlighted PHB's potential for diverse applications due to its biodegradability and reactivity.[51] Hazer and Steinbüchel (2007) reviewed the diversification of PHAs through chemical modifications such as grafting and crosslinking, showing their potential for industrial and medical applications.[52] Hazer et al. (2012) underscored the importance of introducing functional groups through chemical modification to improve PHB's mechanical, thermal, and hydrophilic properties. Such modifications are essential for broadening the applicability of PHB in biomedical fields.[53] Similarly, El-Malek and Steinbüchel (2022) highlighted the significance of chemical and enzymatic modifications in enhancing the sustainability and functionality of PHAs, particularly for medical and therapeutic uses.[54] Domenek et al. (2007) demonstrated the utility of carbodiimide chemistries, such as *N*,*N*′-dicyclohexylcarbodiimide (DCC), for grafting molecules onto PHAs to improve their hydrophilicity and stability.[55] Hazer et al. (2020) highlighted strategies for

https://doi.org/10.1021/acsomega.4c10583
ACS Omega 2025, 10, 12200−12213

modifying PHB to create advanced polymers with enhanced functionality.[56] Borcakli et al. (2003) explored the biosynthesis of PHAs using diverse substrates, showing how structural diversity impacts material properties.[57] Chen (2009) highlighted PHB's potential in drug delivery and bioimplants, emphasizing its biodegradability and biocompatibility.[58] Ashby and Foglia (1998) demonstrated PHB's adaptability for modification through biosynthetic and chemical means.[59] This study integrates these principles using EDC to develop PHB−ectoine NPs with enhanced stability, bioactivity, and multifunctionality for advanced cosmetic applications. These nanoparticles are designed to address the limitations of native PHB and expand its use in the biomedical and cosmetic fields, supported by the comprehensive understanding provided by prior studies.

2. RESULT AND DISCUSSION

2.1. Synthesis of PHB−Ectoine NPs. EDC, a zero-length carboxyl-to-amine crosslinker, was used in the synthesis to facilitate the covalent binding between the carboxylic acid group of PHB and the amine group of ectoine through the formation of an amide bond.[60] Zero-length crosslinkers enable the creation of direct covalent bonds between functional groups without introducing additional spacer molecules into the final product.[61]

In this process, EDC activates the carboxylic group in PHB by generating an *o*-acylisourea intermediate through an ester linkage (Figure 1A). This intermediate compound is highly electrophilic and reacts readily with nucleophiles,[62] such as the secondary amine group in ectoine. The reaction between *o*-acylisourea and ectoine results in the formation of a new PHB−ectoine compound and isourea as a byproduct (Figure 1B).

The use of a zero-length cross-linker ensures that the final PHB−ectoine is formed without any residual linker molecules, preserving the simplicity and integrity of the product structure. EDC is not incorporated into the final product. Additionally, isourea, as a water-soluble by-product of the crosslinking reaction, can be easily removed.[63] The PHB−ectoine NPs were subsequently isolated as a white powder through centrifugation to remove isourea.

2.2. Characterization of PHB−Ectoine NPs. *2.2.1. Functional Groups Analysis of PHB−Ectoine NPs by FTIR.* The FTIR spectra of PHB−ectoine NPs, along with those of standard PHB, ectoine, and rhamnolipid, are presented in Figure 2. The absorption band at 3448 cm^{-1} in the PHB−ectoine NPs spectrum can be attributed to N−H stretching, similar to the 3197 cm^{-1} region observed in the ectoine spectrum, or to terminal O−H groups at the polymer chain ends, which typically exhibit a weak signal around 3439 cm^{-1} in the PHB spectrum.[64,65] However, a precise interpretation must account for potential molecular interactions between the components. The presence of a C═O stretching band at 1663 cm^{-1} indicates the formation of amide bond between PHB and ectoine. The absorption between 1630 and 1680 cm^{-1} is known to be the C═O stretching peak of the amide functional group.[66] If the reaction has occurred, the N−H group of ectoine is expected to have reacted with the carboxyl (−COOH) group of PHB,[67] thereby diminishing the likelihood of a free N−H stretching vibration at 3448 cm^{-1}. Consequently, the 3448 cm^{-1} peak in the PHB−ectoine NPs spectrum is more likely attributed to residual terminal O−H

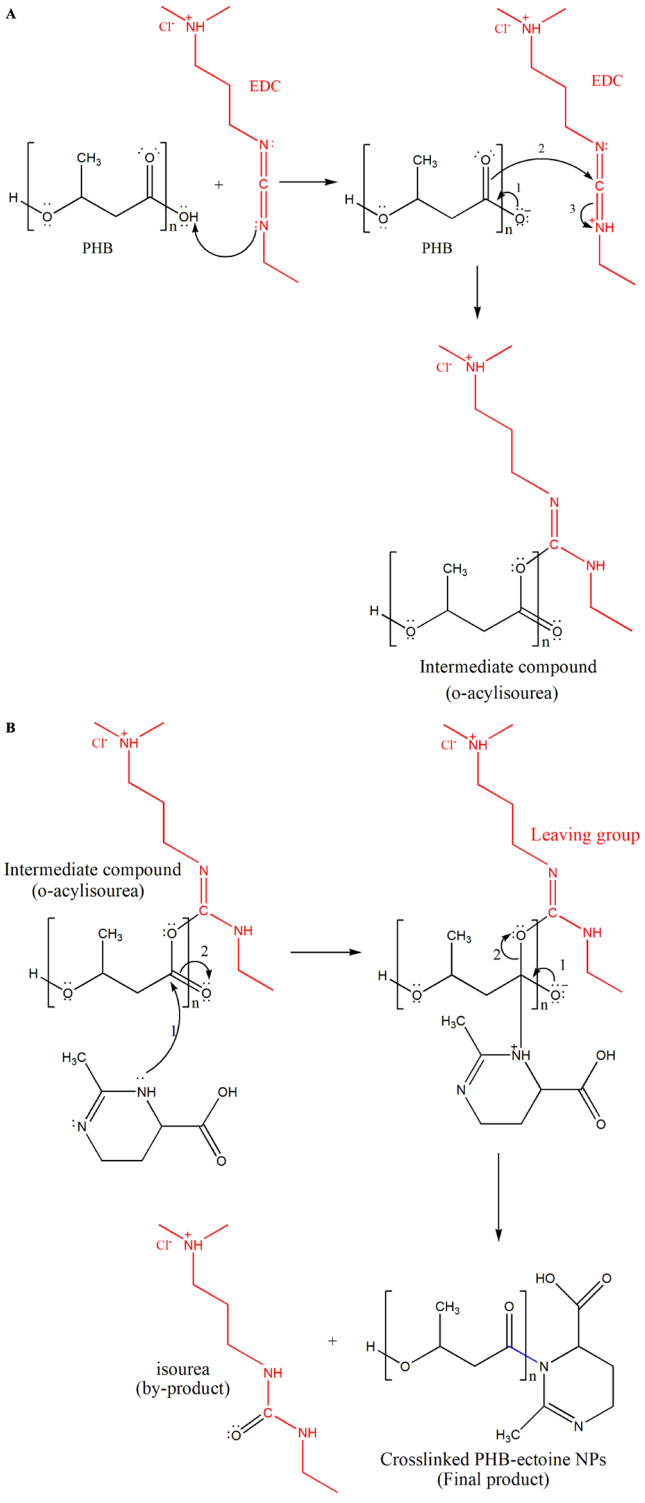

Figure 1. Synthesis reaction of PHB−ectoine NPs. (A) Activation of the carboxyl group in PHB by EDC and (B) formation of PHB−ectoine NPs and the by-product isourea.

groups from PHB or unreacted hydrophilic moieties from ectoine.

The amide absorption peak in the PHB−ectoine NPs spectra is not prominent due to the small number of ectoine compounds that are bound to PHB. Based on the PHB structure, the ectoine is only bound to the end of the PHB polymer chain. These data are supported by the very high C═

https://doi.org/10.1021/acsomega.4c10583
ACS Omega 2025, 10, 12200−12213

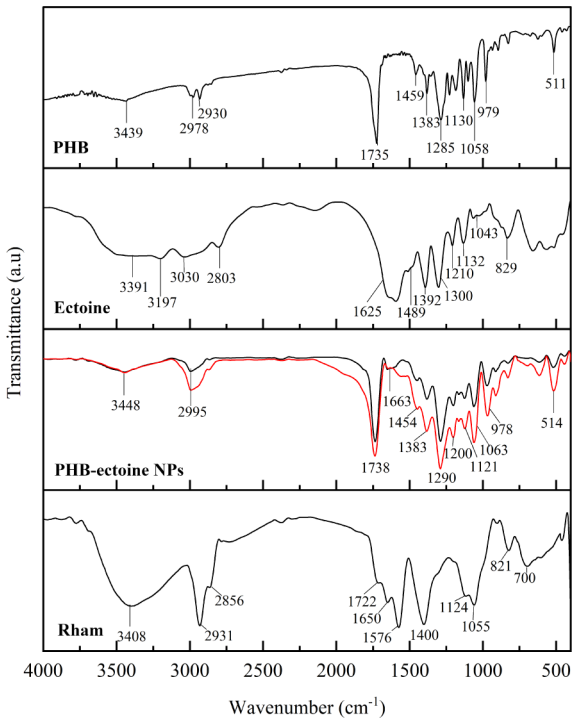

Figure 2. FTIR spectra of PHB, ectoine, PHB-ectoine NPs, and rhamnolipid.

O stretching absorption peak at 1738 cm^{-1}, which indicates the presence of carboxylic acids and aliphatic ketones that resulting in a shift of the amide C═O stretching wavenumber, corresponds to the ectoine and PHB standards at 1625 and 1735 cm^{-1}.[65]

Based on the FTIR spectrum, the typical absorption peaks for each compound are summarized in Table 1. The presence

Table 1. Typical Absorption Peaks of Ectoine Standards, PHB, and PHB-Ectoine NPs

Wavenumbers (cm^{-1})			Vibration mode	Functional groups
Ectoine standard	PHB standard	PHB–ectoine NPs		
3197	-	-	N–H stretching	Amine
3391	3439	3448	O–H	Hydroxyl
3030, 2803	2978, 2930	2995	C–H stretching	$-CH_3$, $-CH_2$
1625	1735	1738	C═O	Carboxylate, aliphatic ketone
-	-	1663	C═O	Amide
1489, 1392	1459, 1383	1454, 1383	C–H bending	$-CH_3$
1300,1210	-	1290, 1200, 1121	C–N stretching	Aromatic amine
-	1285, 1130, 1058	-	C–O–C stretching	Ester

of CH_3 and CH_2 functional groups in PHB–ectoine NPs was observed at 2995 cm^{-1}, corresponding to the CH stretching vibrations at 2978 and 2930 cm^{-1} in standard PHB. These values are also consistent with the CH stretching bands at 2977 and 2934 cm^{-1} previously reported for PHB from *Clostridium hydrogeniformans*.[68]

Additionally, C–H stretching vibrations from the aliphatic methyl and methylene groups within the ectoine ring were observed at 3030 and 2803 cm^{-1}. The presence of C–H bending from CH_3 was identified at 1454 and 1383 cm^{-1}, which corresponds to the characteristic CH_3 bending vibrations observed at 1489 and 1392 cm^{-1} in standard ectoine, as well as 1459 and 1383 cm^{-1} in standard PHB. These results align with the absorption peak at 1485 cm^{-1}, which has been attributed to C–H bending, possibly overlapping with N–H bending.[69]

For further analysis, ectoine, as an amino acid derivative,[31] has typical absorption peaks of the aromatic amine (C–N stretching) at 1300 and 1210 cm^{-1} on the standard spectrum. These absorption peaks also appeared at 1290–1121 cm^{-1} in PHB–ectoine NPs. Meanwhile, PHB is a polymer resulting from the condensation of alcohol with carboxylic acid,[70] which has a typical absorption peak of the C–O–C ester at 1285–1058 cm^{-1} on the standard spectrum. FTIR analysis showed that the synthesized PHB–ectoine NPs were successfully bound, although they needed to be optimized.

To ensure the compatibility of the rhamnolipid–PHB–ectoine nanoformulation, PHB–ectoine NPs were dispersed in rhamnolipid solutions. The dispersion was stirred for 1 h, after which the NPs were separated from the rhamnolipid solution through centrifugation. The collected NPs were then freeze-dried, and their structural properties were analyzed using FTIR. Unexpectedly, the rhamnolipid did not alter the PHB–ectoine NPs, as indicated by the red spectrum. Additionally, the typical absorption peak of rhamnolipid at 1124 cm^{-1}, which signifies the C–O stretching of carbohydrates,[71] did not appear in the red spectrum. The analysis results suggest that PHB–ectoine NPs do not bind directly to rhamnolipids but interact through non-covalent bonds.

2.2.2. Structure Analysis of PHB–Ectoine NPs by ^{1}H NMR. The ^{1}H NMR spectrum of the PHB–ectoine sample measured in the CD_3OD solvent shows chemical shift patterns that match the expected structure, as shown in Figure 3. In the low-field region (1.0–1.3 ppm), strong signals are observed, corresponding to protons from the methyl groups in the aliphatic chain of PHB. Additionally, the signal around 2.1 ppm is attributed to methylene protons, consistent with the chemical shifts of 1.2 and 2.5 ppm reported for CH_3 and CH_2 protons along the PHB backbone in*Pseudomonas mandelii* CBS-1.[72] This signal may also represent CH_2 groups in the ectoine ring, as observed at 2.0–2.1 ppm in ectoine spectra from halophilic bacteria.[73] The methine proton in PHB appears at 4.8–4.9 ppm, similar to the 5.3 ppm shift reported for PHB spectra from*Pseudomonas plecoglossicida*.[74] This proton is part of the CH group on a chiral carbon attached to a hydroxyl group, which causes deshielding and typically places it in the 4.8–5.2 ppm range.[75]

The ^{1}H-NMR spectra of PHB–ectoine were compared to those of standard ectoine (Figure 4) to assess structural consistency. In the standard ectoine spectra, significant peaks were observed at higher chemical shifts, including a singlet at 2.1 ppm, which corresponds to the methyl protons of the ectoine ring. Similarly, the PHB–ectoine spectra displayed a singlet at 2.2 ppm, indicating the retention of this characteristic structural feature. Peaks in the 3.1–4.0 ppm region in the standard ectoine spectra, attributed to protons bonded to heteroatoms such as those in carboxylate groups or near nitrogen, were also present in the PHB–ectoine spectra within the same range, specifically at 3.3–4.0 ppm. This overlap

https://doi.org/10.1021/acsomega.4c10583
ACS Omega 2025, 10, 12200–12213

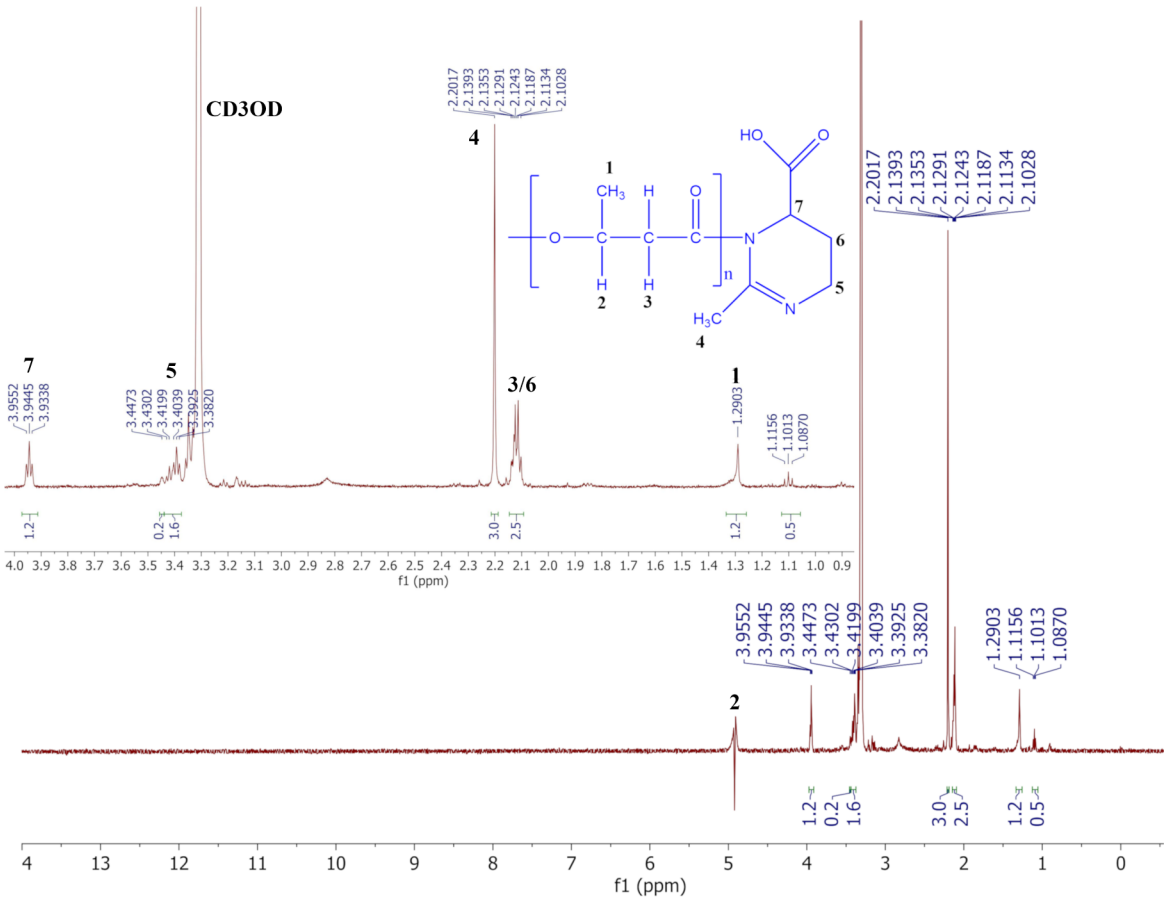

Figure 3. ^{1}H NMR spectra of the PHB−ectoine NPs.

confirms that the heteroatom-related proton environments are preserved in the PHB−ectoine complex. Notably, major chemical shifts have been reported at 2.21, 3.43, and 4.05 ppm in the ectoine spectra from*E. coli*,[76] further supporting structural alignment.

Additionally, D_2O was used as the solvent for the standard ectoine spectra, with characteristic solvent peaks observed at 4.6−4.8 ppm due to deuterium. In contrast, CD_3OD was used as the solvent for the PHB−ectoine spectra, showing a solvent peak at 3.31 ppm, corresponding to deuterated methanol. These align with the solvent residual peaks of D_2O and CD_3OD reported by Babij et al. (2016) at 4.79 and 3.31 ppm.[77] Importantly, no significant peaks outside the relevant chemical shift range were observed in the PHB−ectoine spectra, indicating the absence of major impurities.

2.2.3. Morphological and Element Analysis of PHB−Ectoine NPs by SEM-EDX and TEM Imaging. The morphology and element composition of PHB−ectoine NPs were characterized by SEM-EDX analysis.[78] The PHB−ectoine NPs were found to have a more homogeneous spherical shape (Figure 5A). In contrast, the standard PHB, according to Rizki et al. (2023), appears to have a slightly irregular spherical shape.[65] Similar findings were reported by Corrado et al. (2022), indicating that PHB-loaded nanoparticles have a spherical shape with an irregular surface.[79] The incorporation of ectoine into PHB particles alters the morphological shape of the PHB (Figure 5B). PHB−ectoine NPs display two distinct layers, highlighted by arrows in Figure 5C. Further analysis is necessary to determine the composition of these inner and outer layers. However, previous studies have demonstrated PHB's ability to load active compounds, such as curcumin[80] and astaxanthin.[21] Additionally, Figure 5D displays the morphology of rhamnolipid−PHB−ectoine nanoformulation. Rhamnolipid appears to be concentrated around the PHB−ectoine particles. Supported by FTIR and PSA analysis, rhamnolipid seems to reduce the size of PHB−ectoine NPs without affecting their structure.

Further results with EDX analysis show that PHB−ectoine NPs consist of 95.17% (mass) carbon (C), 4.41% (mass) oxygen (O), and 0.41% (mass) nitrogen (N). Research by Rizki et al. (2023), which used the same standard PHB, shows that PHB itself consists of 63.58 ± 0.06% (mass) carbon (C) and 36.42 ± 0.31% (mass) oxygen (O).[65] The presence of nitrogen, which is found only in ectoine in the PHB−ectoine NPs, confirms the successful covalent bonding of ectoine to PHB.

2.2.4. Particle Size Analysis of PHB−Ectoine NPs. The synthesized PHB−ectoine NPs exhibited a less homogeneous size distribution in water, ranging from 500 to 2500 nm. The particle size distribution peaked at 950 nm, with an average size of 1280 ± 610 nm (Figure 6A). The polydispersity index (PI) of PHB−ectoine NPs in water was 0.574, indicating a broad size distribution and potential particle aggregation. Meanwhile, in rhamnolipid solution (Figure 6B), the particle size was reduced to a range of 247−946 nm, with a peak at 455 nm and an average size of 527 ± 228 nm, along with a lower PI of 0.291, suggesting improved dispersion stability. The size of the particles influences the balance between van der Waals attraction and electrostatic repulsion, which is critical for maintaining dispersion stability. Smaller particles, with a higher

https://doi.org/10.1021/acsomega.4c10583
ACS Omega 2025, 10, 12200−12213

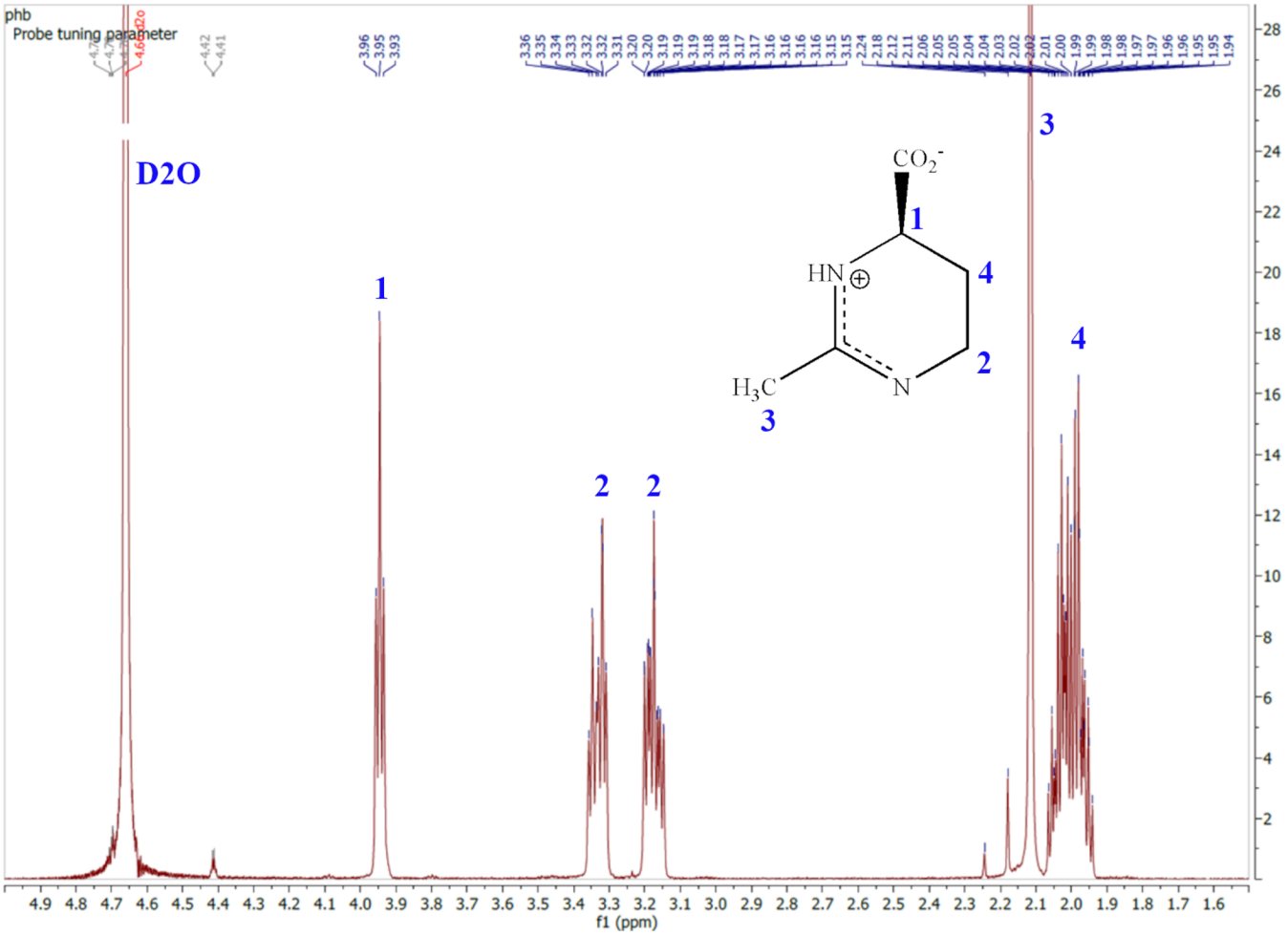

Figure 4. ^{1}H NMR spectra of the ectoine standard.

surface-to-volume ratio, benefit more from electrostatic repulsion to maintain stability compared to larger particles.[81] Previous research has demonstrated that rhamnolipid can lower surface tension in cosmetic formulations, making it suitable for stabilizing suspensions in various applications.[82] Therefore, the combination of PHB−ectoine NPs with rhamnolipid has significant potential for use in skin care products.

2.2.5. Zeta Potential Analysis of PHB−Ectoine NPs. The surface charge properties and stability dispersion of the PHB−ectoine NPs were characterized by zeta potential analysis in distilled water at pH ±7. The zeta potential of PHB−ectoine NPs is −61.47 ± 0.64 mV, greater than −45.10 ± 1.00 mV for PHB−liposome that has been reported.[25] PHB has an isoelectric point of 5.4, which has a positively charged surface in pH below 6.[83] In PHB−ectoine NPs, the carboxylate group of PHB forms an amide bond with ectoine; therefore, PHB does not contribute to the charge. The level of negative charge on PHB−ectoine NPs reflects the role of ectoine in providing this charge. Ectoine in the PHB−ectoine NPs structure contains a carboxylate group. It has been known that the isoelectric point of ectoine is 3.2, so it also has a negative charge at pH 7.[84] Nanoparticles with zeta potential values higher than +30 mV and lower than −30 mV are reported to have higher stability.[85]

2.3. In Vitro Skin Protective Study of PHB−Ectoine NPs. *2.3.1. Anti-Irritation Effectiveness.* An anti-irritation assay was carried out to determine the ability of PHB−ectoine NPs in protecting skin proteins from surfactants commonly found in cosmetic products, such as SDS and rhamnolipid. The zein protein used is a maize protein from the prolamin group,[86] which has a globular structure similar to the keratin protein that is not soluble in aqueous solution unless it is denatured.[87] This protein serves as an indicator of the potential denaturation of keratin due to surfactant exposure. Figure 7 shows the diagram of the anti-irritation activity of PHB and PHB−ectoine NPs using SDS and rhamnolipid as irritant agents. The data are presented as the mean ± standard deviation (SD), with experiments performed in triplicate to ensure reliability and reproducibility.

Initially, a 1% (w/v) solution of SDS and rhamnolipid could denature zein protein by 53.01% and 29.70%, respectively. The difference in percentage denaturation indicates that rhamnolipid has non-irritating properties compared to SDS.[88] The inclusion of PHB dispersant at concentrations ranging from 0.5% to 1.2% (w/v) proved to be ineffective in protecting the zein protein from the SDS and rhamnolipid solution. The zein protein remained denatured by 38.32−46.63% when exposed to SDS and by 14.07−24.82% when exposed to rhamnolipid. These findings indicate that PHB does not have anti-irritant properties and also did not provide a significant effect on the irritant activity of SDS and rhamnolipid.

The prepared nanoparticles exhibited superior anti-irritation efficacy compared to PHB. Incorporating 0.5−1% (w/v)

https://doi.org/10.1021/acsomega.4c10583
ACS Omega 2025, 10, 12200−12213

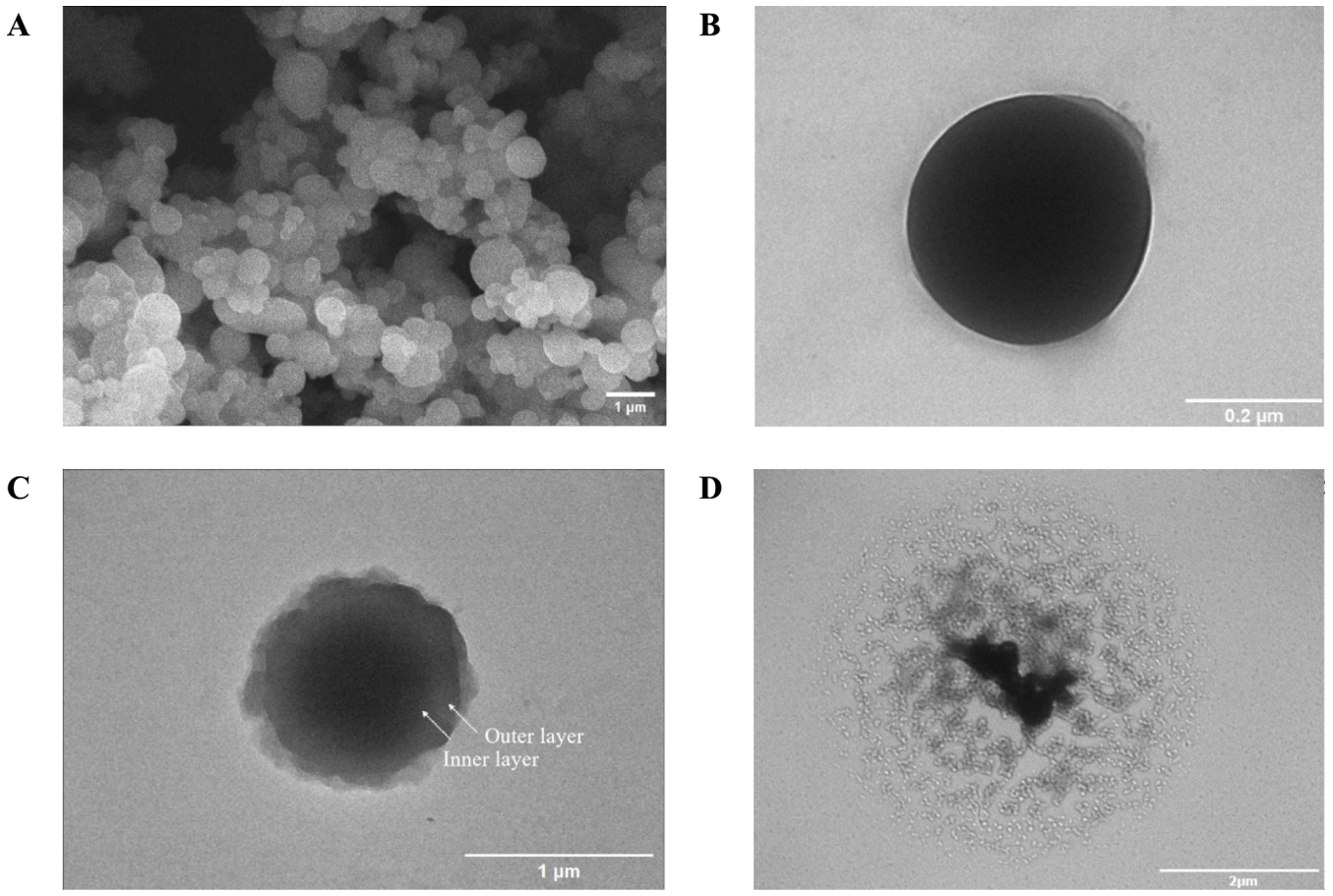

Figure 5. SEM image of (A) PHB−ectoine NPs (×10,000 magnification). TEM image of (B) PHB (×40,000 magnification), (C) PHB−ectoine NPs (×10,000 magnification), and (D) rhamnolipid−PHB−ectoine nanoformulation (×5,000 magnification).

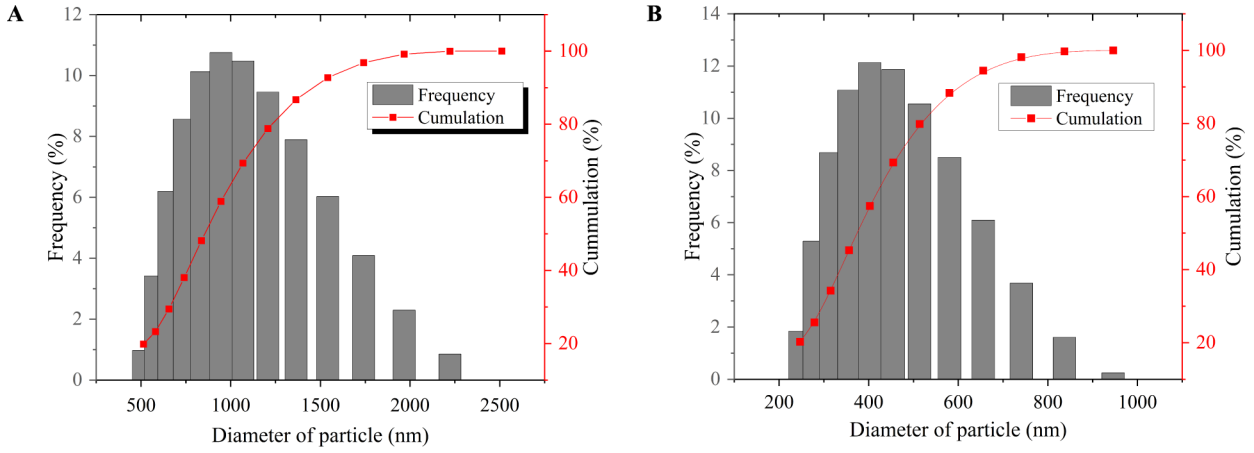

Figure 6. Particle size distribution of PHB−ectoine NPs in (A) water and (B) rhamnolipid solution.

PHB−ectoine NPs dispersant resulted in a reduction of zein protein denaturation to 3.23−16.2% and 3.50−55.86% when exposed to SDS (Figure 7A) and rhamnolipid (Figure 7B) solutions. In contrast to the SDS solution findings, the incorporation of 0.5% (w/v) PHB−ectoine NPs results in an elevation of the irritant potency of the rhamnolipid. Nonetheless, the optimal concentration for achieving the highest anti-irritation activity was found to be 1% (w/v), where PHB−ectoine NPs effectively suppressed protein denaturation to 3.23 and 3.50%, providing protection for zein protein by 96.77 and 96.5% against SDS and rhamnolipid. However, increasing the concentration of PHB−ectoine to higher levels (1.2% w/v) resulted in diminished effectiveness in protecting proteins from SDS and rhamnolipid, with 37.79 and 5.57% of zein protein denatured, respectively.

In 2020, Bujak et al. reported that the introduction of ectoine into anionic surfactants decreases the irritant effects of sodium lauryl sulfate (SLS), sodium coco sulfate (SCS), sodium laureth sulfate (SLES), and sodium lauroyl sarcosinate (SARKO). That finding aligns with the outcomes of this study, which demonstrate ectoine's capability to enhance the anti-irritation properties of PHB from both synthetic and

https://doi.org/10.1021/acsomega.4c10583
ACS Omega 2025, 10, 12200−12213

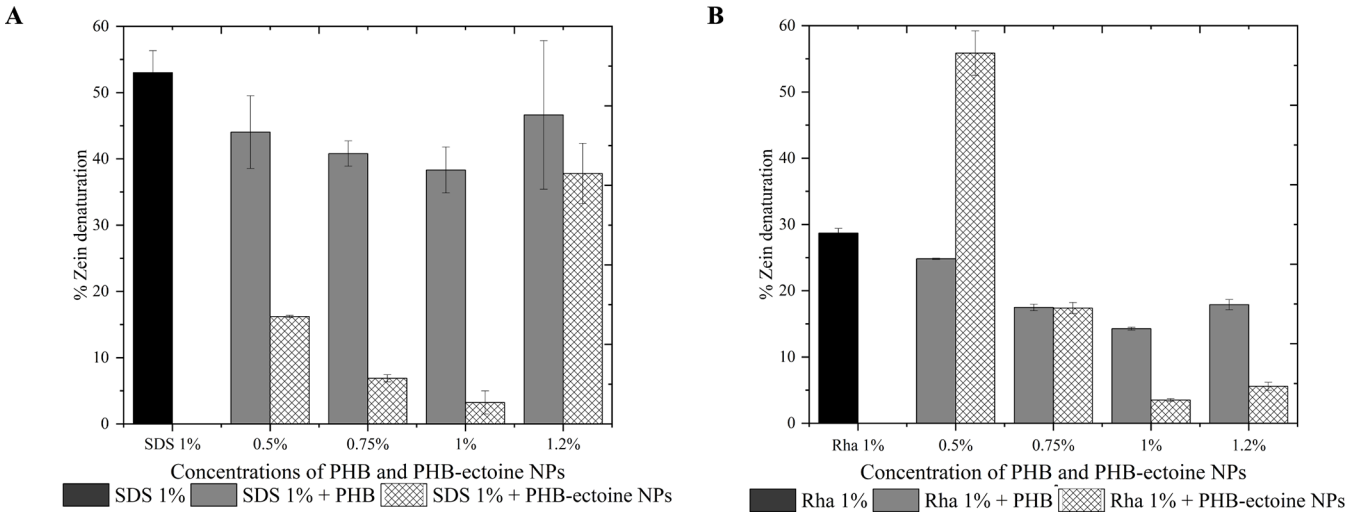

Figure 7. Anti-irritation effectiveness diagram of PHB and PHB−ectoine NPs using (A) SDS (1% w/v) and (B) Rha (rhamnolipid) (1% w/v) as irritating agent.

biosurfactant exposure. The inclusion of ectoine in the PHB structure enhances its safety profile for cosmetic applications, as it diminishes its irritant potential.[89] Furthermore, this research suggests that rhamnolipid could serve as a gentler alternative to synthetic surfactants in cosmetics due to its potential as a biosurfactant.

2.3.2. Anti-UVB Activity (SPF Measurements). The anti-UVB activity was assessed by determining the sun protection factor (SPF) value, which previous researchers have validated as a measure of sunscreen's effectiveness against UVB radiation.[90] In this study, PHB demonstrated an SPF of 4.19 ± 0.17, offering approximately 76.2% protection against UVB rays. Covalent binding of PHB with ectoine enhanced this protection to 82.3%. The synthesized PHB−ectoine NPs complex exhibited an SPF of 5.64 ± 0.30, consistent with earlier findings that highlight PHB's ability to scatter UVB rays and boost the SPF of other compounds it binds to.[25] Further analysis involving the addition of rhamnolipid into PHB−ectoine NPs led to a slight reduction in SPF to 5.06 ± 0.24, although the protection level remained around ±80%. A summary of all SPF test results is presented in Table 2, where

Table 2. Anti-UVB Test Results

Sample	SPF	% UVB protection
PHB	4.19 ± 0.17	76.2
Ectoine	1.61 ± 0.19	38.0
PHB−ectoine NPs	5.64 ± 0.30	82.3
Rhamnolipid	1.26 ± 0.16	20.4
Rhamnolipid−PHB−ectoine nanofluid	5.06 ± 0.24	80.2

SPF values are reported as mean ± standard deviation (SD), with experiments conducted in triplicate. These findings suggest that PHB−ectoine NPs show significant potential as an anti-UVB agent, even when formulated as a nanofluidic with rhamnolipid.

PHB−ectoine NPs exhibit the highest SPF value, highlighting the significant role of PHB within the nanoparticles, where its UVB protection ability remains well preserved. The mechanism behind UVB absorption typically involves electron transitions, as the photon energy from UVB radiation is sufficient to excite electrons. Structurally, PHB contains a C═O functional group with electrons in the π and nonbonding (n) orbitals, which are capable of absorbing UV light in the 200−300 nm range.[91] Furthermore, the covalent binding of PHB with ectoine, forming an amide bond, enhances UVB absorption, as the electrons in the C═O group of amide bonds can also transition from the π and n orbitals to the π^* orbital. This explains why the SPF value of PHB−ectoine NPs is higher than that of PHB.

UVB radiation can be highly dangerous. Previous in vivo studies have shown that UVB radiation can affect the morphology of the epidermal layer of the skin, disrupt the permeability barrier system,[92] cause morphological changes in the lipids of the stratum corneum,[93] increase transepidermal water loss, and reduce skin hydration.[94] In this context, the prepared PHB−ectoine NPs can serve a dual function by blocking UVB rays while simultaneously hydrating the skin.

2.3.3. Antibacterial Activity. Gram-positive (*S. aureus*) and Gram-negative (*E. coli*) bacterial strains were utilized to assess antibacterial activity using the well diffusion method. The two bacterial strains were chosen due to their frequent involvement in various skin-mediated infections.[95] Notably, PHB−ectoine NPs (10 mg/mL) demonstrated no antibacterial activity on both bacterial strains (Figures 8A and 10A). This finding aligns with the notion that ectoine possesses a robust capacity to bind water, forming a hydro-ectoine complex that can shield bacterial cells.[32] Conversely, rhamnolipid (10 mg/mL) exhibited antibacterial activity against*S. aureus* (Figure 8B). Specifically, rhamnolipid inhibited the growth of*S. aureus* bacteria by 515 ± 48 mm^2, surpassing previous findings at the same concentration, which reported an inhibition zone of 283 mm^2.[96] The inclusion of rhamnolipid as a dispersant conferred an antibacterial property to the PHB−ectoine NPs against*S. aureus* bacteria. These findings are in line with prior studies indicating the efficacy of rhamnolipids in controlling the growth of*S. aureus*.[97]

Figure 9 depicts the findings of a study evaluating the antibacterial activity of rhamnolipid−PHB−ectoine nanoformulation against*S. aureus*, where the concentration of PHB−ectoine NPs was varied to 5, 10, and 20 mg/mL. The data presented in Figure 9 represent mean values ± standard deviation (SD) from three independent experiments to ensure reproducibility and accuracy. Variability in inhibition zone

https://doi.org/10.1021/acsomega.4c10583
ACS Omega 2025, 10, 12200−12213

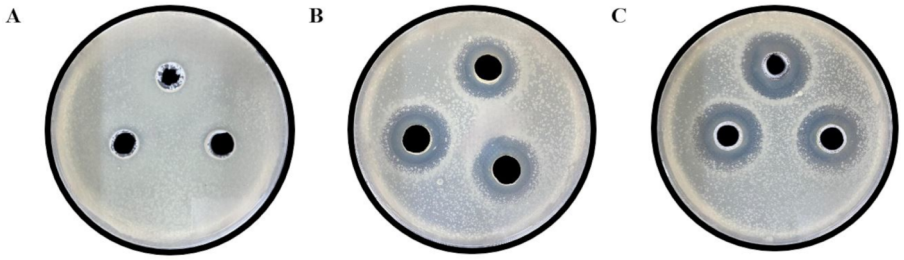

Figure 8. Antibacterial activity test results against*S. aureus* of (A) PHB−ectoine NPs (10 mg/mL), (B) rhamnolipid (10 mg/mL), and (C) nanofluid (PHB−ectoine NPs 5 mg/mL and rhamnolipid 10 mg/mL).

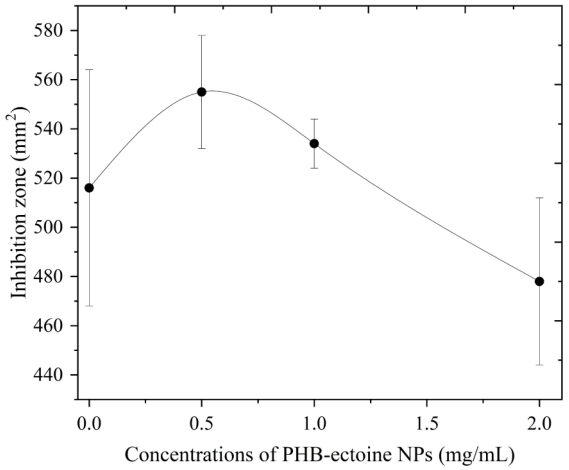

Figure 9. Optimization results of PHB−ectoine NPs concentration in nanofluids against*S. aureus*.

sizes may result from uneven antimicrobial diffusion, unstable PHB−ectoine dispersion, inconsistent microbial growth, and agent stability.[98] Furthermore, particle size analysis (PSA) confirms a non-uniform size distribution of PHB−ectoine NPs, influencing diffusion rates and bacterial interactions, thereby affecting inhibition zone measurements.[99]

However, at a concentration of 5 mg/mL, the nanofluid displayed the highest antibacterial effectiveness (Figure 8C), with an inhibition zone of 554 ± 22 mm^2, surpassing the antibacterial activity of rhamnolipid itself. Meanwhile, PHB−ectoine NPs at concentrations of 10 and 20 mg/mL resulted in inhibition zones of 534 ± 10 and 478 ± 34 mm^2, respectively. This underscores the capability of rhamnolipid to enhance the antibacterial activity of PHB−ectoine in nanofluid form.*S. aureus* is a common bacterium that lives on the skin and is the most abundant skin-colonizing organism that causes skin infections.[100] The ability of PHB−ectoine NPs to boost the antibacterial properties of rhamnolipids against this bacterium holds promise for applications in the cosmetics industry.

Unlike the antibacterial activity observed against *S. aureus*, rhamnolipid (Figure 10B) and nanofluids (Figure 10C) exhibited no antibacterial effects against*E. coli*. According to a study by Ferreira et al. (2019), rhamnolipid demonstrates resistance to Gram-negative bacteria, such as *E. coli* and *Salmonella enterica*, across different pH levels.[97] This resistance is attributed to the protective outer membrane of Gram-negative bacteria, which acts as a barrier that impedes the antimicrobial action of the rhamnolipid. This outer membrane effectively shields the bacteria from the effects of rhamnolipid, rendering it ineffective against these organisms.[101]

3. CONCLUSION

The PHB−ectoine nanoparticles were successfully synthesized using a straightforward solvation method, with EDC serving as the cross-linking agent. FTIR analysis confirmed the formation of an amide bond, indicated by an absorption peak at 1663 cm^{-1}. SEM images revealed that the PHB−ectoine NPs had a homogeneous spherical shape, composed of carbon, oxygen, and nitrogen elements. TEM imaging further verified encapsulation by two distinct layers, resulting in a zeta potential of −61.47 ± 0.64 mV. These characterizations confirmed the successful binding of PHB and ectoine molecules. Additionally, in vitro analysis of the skin-protective properties of PHB−ectoine NPs demonstrated notable anti-irritant, SPF, and antibacterial activities. The nanoparticles effectively protected and maintained the integrity of zein protein when exposed to 1% (w/v) SDS and rhamnolipids, showing a significantly higher anti-irritant potential than PHB alone. Moreover, the PHB−ectoine NPs exhibited SPF activity with an SPF of 5.64 ± 0.30, offering 82.3% UVB protection. Antibacterial tests indicated that the rhamnolipid−PHB−ectoine nanoformulation was capable of inhibiting the growth of*S. aureus*.These results underscore the potential of incorporating PHB−ectoine NPs with rhamnolipid as an active

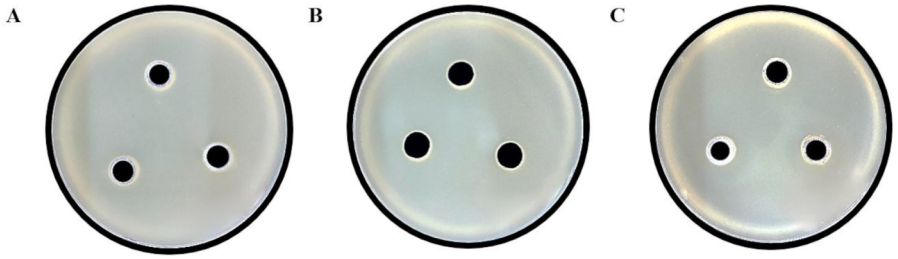

Figure 10. Antibacterial activity test results against *E. coli* of (A) PHB−ectoine NPs (10 mg/mL), (B) rhamnolipid (10 mg/mL), and (C) nanofluid (PHB−ectoine NPs 10 mg/mL and rhamnolipid 10 mg/mL).

https://doi.org/10.1021/acsomega.4c10583
ACS Omega 2025, 10, 12200−12213

Table 3. EE.I Constant Value at UVB Wavelengths

No.	1.	2.	3.	4.	5.	6.	7.
λ [nm]	290	295	300	305	310	315	320
EE.I	0.015 ± 0	0.081 ± 7	0.287 ± 4	0.327 ± 8	0.186 ± 4	0.083 ± 7	0.018 ± 0

ingredient, offering anti-irritant, antibacterial, and UVB protection, especially in cosmetic formulations.

4. MATERIALS AND METHODS

4.1. Materials. Ethanol (C_2H_5OH, 95−97%), distilled water, EDC ($C_8H_{17}N_3$·HCl), rhamnolipid ($C_{32}H_{58}O_{13}$), Zein protein, sodium dodecyl sulfate (SDS), and Mueller Hinton Agar were purchased from Sigma-Aldrich (p.a.). Furthermore, ectoine ($C_6H_{10}N_2O_2$) and PHB ($[COCH_2CH(CH_3)O]_n$) were obtained from natural origin and were distributed by Sigma-Aldrich.

4.2. Methods. *4.2.1. Synthesis of PHB−Ectoine NPs.* The PHB−ectoine NPs were synthesized using a straightforward solution process mediated by an EDC crosslinking agent at 45 °C. Initially, 500 mg of PHB was dissolved in 100 mL of ethanol and homogenized at room temperature for 90 min. Crosslinking of the particles was induced by adding 100 mg of EDC, which acts by activating the carboxyl groups on the particles. This activation allows the particles to react with amine groups, forming covalent bonds and resulting in the formation of crosslinked networks. Ectoine, which contains amine groups, was then added dropwise at a constant flow rate of 1 mL/min, and the mixture was allowed to react overnight under stirring at 150 rpm and 45 °C. After the reaction, the nanoparticles were collected by centrifugation at 5000 rpm for 30 min and freeze-dried for further analysis.[102]

4.2.2. Dispersing of PHB−Ectoine NPs in Rhamnolipid Solutions. The rhamnolipid solution was prepared by dissolving rhamnolipid particles in distilled water, followed by homogenization through stirring at 150 rpm for 15 min. The PHB−ectoine NPs were then added to the rhamnolipid solution and further homogenized until a stable dispersion was achieved.[103]

4.2.3. PHB−Ectoine NPs Characterization. 4.2.3.1. FTIR Analysis. The functional groups and the presence of amide bonds in PHB-ectoine NPs were confirmed using Fourier transform infrared spectroscopy (FTIR) with a Prestige 21 instrument (Shimadzu, Japan). The PHB−ectoine NPs were prepared into KBr pellets using a vacuum compression pump, and the FTIR spectrum was recorded in the range of 500−4000 cm^{-1}.[104]

4.2.3.2. ^1H NMR Analysis. The structures of PHB−ectoine NPs and ectoine standard were recorded with an Agilent DD2 spectrometer system operating at 500 MHz, using residual and deuterated solvent peaks as reference standards.[105]

4.2.3.3. SEM-EDX Analysis. The composition and surface morphology of PHB−ectoine NPs were analyzed using Scanning Electron Microscopy coupled with Energy-Dispersive X-ray Spectroscopy (SEM-EDX) (JSM-6510A/JSM-6510LA, JEOL Ltd., Japan). The sample was prepared by coating the nanoparticles with a thin layer of gold on a carbon adhesive plate, using a current of 10 mA for 20 min. Composition analysis was conducted with an EDX detector, and the surface morphology was observed at a magnification ranging from 10,000× to 20,000×.[106]

4.2.3.4. TEM Analysis. The internal structure of PHB−ectoine NPs was analyzed using Transmission Electron Microscopy (TEM) with an acceleration voltage of 100 kV. A sample of PHB−ectoine NPs (1 mg/mL in distilled water) was prepared by sonication for 15−20 min. A small amount of the sample was then placed in the observation area. High-resolution images of the nanoparticles were obtained at magnifications ranging from 5,000× to 40,000× using an electron beam.[107]

4.2.3.5. Particle Size Analysis. Particle size analysis was conducted on water and rhamnolipid dispersions. To prepare the sample, PHB−ectoine NPs were dispersed in water and rhamnolipid to create a nanofluid with a concentration of 10 mg/mL. This mixture was then analyzed using a Particle Size Analyzer (PSA) to determine the particle size distribution. Data processing involved plotting the particle size diameter against both frequency and cumulative amounts.[108]

4.2.3.6. Zeta-Potential Analysis. The zeta potential of PHB−ectoine NPs was analyzed using Dynamic Light Scattering (DLS) with a Horiba SZ-100 Nanoparticle Analyzer (Osaka, Japan). The analysis was performed by dispersing the nanoparticles in distilled water at a concentration of 5 mg/mL and at a pH of 7.[84]

4.2.4. In Vitro Skin Protection Study of PHB−Ectoine Nps. 4.2.4.1. Anti-Irritation Effectiveness. The anti-irritation effectiveness was assessed gravimetrically using zein protein as a skin protein model, following a modified method from Cohen et al., 2016. In this process, 0.25 grams of zein protein were dissolved and stirred in 5 mL of PHB−ectoine NPs at concentrations of 0.5%, 0.75%, 1%, and 1.2% (w/v in distilled water) for 5 min. To induce irritation, 5 mL of SDS and rhamnolipid (1% w/v in distilled water) were added, and the mixture was stirred at 150 rpm for 60 min. The undenatured zein protein residue was filtered through vacuum filtration and dried overnight at 37 °C. The anti-irritation effectiveness was calculated as the percentage of denatured zein protein using the following eq 1 below:

$$\%\ \text{zein denatured} = [\text{Total zein added to the solution}(\pm 0.25\text{g}) - \text{Total zein(g)after drying}] / [\text{Total zein added to the solution}(\pm 0.25\text{g})] \times 100 \quad (1)$$

For samples dispersed in distilled water, the percentage of denatured zein must be calculated by subtracting the total amount of sample (in grams) added to the solution. All procedures were conducted in triplicate, and the anti-irritation effectiveness of PHB standards was also evaluated for comparison.[109]

4.2.4.2. Anti-UVB Activity (SPF Measurement). The prepared PHB−ectoine NPs were dissolved in ethanol (96% v/v) to a concentration of 200 μg/mL. The absorbance of this solution was measured within the wavelength range of 290−320 nm, with ethanol (96% v/v) serving as the blank. The Sun Protection Factor (SPF) or anti-UVB activity was then calculated using the Mansur eq 2 below:

$$\text{SPF} = \text{CF} \times \sum_{290}^{320} \text{EE}(\lambda) \times I(\lambda) \times \text{Abs}(\lambda) \quad (2)$$

https://doi.org/10.1021/acsomega.4c10583
ACS Omega 2025, 10, 12200−12213

Where CF is the correlation factor (10); EE (λ) represents erythema effectiveness; $I(\lambda)$ denotes solar intensity; and Abs(λ) is the absorbance measured for PHB−ectoine NPs at UVB wavelengths. The EE.I values are constant and are presented in Table 3 as the mean ± standard deviation.[110] SPF measurements were replicated three times. Ectoine, PHB, and rhamnolipid standards were also studied for further comparison. For all the obtained SPF value, the percentages of protection are measured using the following eq 3:

$$\%\text{UVB protection} = \left(1 - \frac{1}{\text{SPF}}\right) \times 100\% \quad (3)$$

4.2.4.3. Antibacterial Activity. The antibacterial activity was assessed against *S. aureus* and *E. coli* by measuring the inhibition zone using the well diffusion method. The sample formulations tested in this study are given in Table 4.

Table 4. Nanofluids Formulation for the Antibacterial Activity Assay

Sample No.	1	2	3	4	5
PHB−ectoine NPs (mg/mL)	10	0	5	10	20
Rhamnolipid (mg/mL)	0	10	10	10	10

Specifically, the bacterial suspension with a concentration equivalent to McFarland 0.5 was added to Mueller−Hinton Agar (MHA) medium at a temperature of 30−35 °C. The mixture was then poured into plates to form the agar layer. Wells were created in the agar layer, and 100 μL of the sample was added to each well. The plates were incubated at 37 °C for 12−16 h. The area of the inhibition zone that formed was then measured and recorded.[111]

■ ASSOCIATED CONTENT

Supporting Information

The Supporting Information is available free of charge at https://pubs.acs.org/doi/10.1021/acsomega.4c10583.

Additional experimental data on in vitro skin protective study of PHB−ectoine NPs Raw images of antibacterial activity (PDF)

■ AUTHOR INFORMATION

Corresponding Author

Rukman Hertadi − *Biochemistry and Biomolecular Engineering Research Division, Faculty of Mathematics and Natural Sciences, Bandung Institute of Technology, Bandung 40132, Indonesia;* orcid.org/0000-0002-4352-5830; Phone: +62-222515032; Email: rhertadi@itb.ac.id; Fax: +62-222502360

Authors

Alma Tyara Simbara − *Biochemistry and Biomolecular Engineering Research Division, Faculty of Mathematics and Natural Sciences, Bandung Institute of Technology, Bandung 40132, Indonesia;* orcid.org/0009-0006-7574-2502

Fera Faridatul Habibah − *Biochemistry and Biomolecular Engineering Research Division, Faculty of Mathematics and Natural Sciences, Bandung Institute of Technology, Bandung 40132, Indonesia;* orcid.org/0000-0003-2630-2894

Complete contact information is available at: https://pubs.acs.org/10.1021/acsomega.4c10583

Author Contributions

A.T.S.: Conceptualization, methodology, validation, formal analysis, investigation, writing-original draft, writing-review and editing, and visualization. F.F.H.: Conceptualization, methodology, investigation, and writing-review and editing. R.H.: Conceptualization, methodology, validation, resources, writing-review and editing, supervision, project administration, and funding acquisition.

Notes

The authors declare no competing financial interest.

■ ACKNOWLEDGMENTS

We gratefully acknowledge the Department of Chemistry, Faculty of Mathematics and Natural Sciences, Bandung Institute of Technology, for providing the facilities and resources necessary to conduct this research. We are also grateful to the Center for Chemical Instrumentation, Faculty of Mathematics and Natural Sciences, Bandung Institute of Technology, for their support in recording the NMR data.

■ REFERENCES

(1) McKnight, G.; Shah, J.; Hargest, R. Physiology of the skin. *Surgery* **2022**, *40*, 8−12.

(2) Eyerich, S.; Eyerich, K.; Traidl-Hoffmann, C.; Biedermann, T. Cutaneous barriers and skin immunity: Differentiating a connected network. *Trends Immunol.* **2018**, *39*, 315−327.

(3) Sparr, E.; Millecamps, D.; Isoir, M.; Burnier, V.; Larsson, Å.; Cabane, B. Controlling the hydration of the skin though the application of occluding barrier creams. *J. R. Soc. Interface* **2013**, *10*, 20120788.

(4) Romanovsky, A. A. Skin temperature: Its role in thermoregulation. *Acta. Physiol.* **2014**, *210*, 498.

(5) Mostafa, W. Z.; Hegazy, R. A. Vitamin D and the skin: Focus on a complex relationship: A review. *J. Adv. Res.* **2015**, *6*, 793−804.

(6) Trompette, A.; Pernot, J.; Perdijk, O.; Alqahtani, R. A. A.; Domingo, J. S.; Camacho-Muñoz, D.; Wong, N. C.; Kendall, A. C.; Wiederkehr, A.; Nicod, L. P.; et al. Gut-derived short-chain fatty acids modulate skin barrier integrity by promoting keratinocyte metabolism and differentiation. *Mucosal Immunol.* **2022**, *15*, 908−926.

(7) Kuchangi, S. N.; Mruthunjayappa, M. H.; Kotrappanavar, N. S. An overview of water pollutants in present scenario. In *3D printing technology for water treatment applications*, Pandey, J. K.; Manna, S.; Patel, R. K., Eds.; Elsevier Inc: Amsterdam, 2023, pp. 83−105.

(8) Gupta, S.; Sharma, S.; Nadda, A. K.; Husain, M. S. B.; Gupta, A. Biopolymers from waste biomass and its applications in the cosmetic industry: A review,. *Mater. Today: Proc.* **2022**, *68*, 873−879.

(9) Goyal, N.; Jerold, F. Biocosmetics: Technological advances and future outlook. *Environ. Sci. Pollut. Res.* **2023**, *30*, 25148.

(10) Panico, A.; Serio, F.; Bagordo, F.; Grassi, T.; Idolo, A.; de Giorgi, M.; Guido, M.; Congedo, M.; de Donno, A. Skin safety and health prevention: An overview of chemicals in cosmetic products. *J. Prev. Med. Hyg.* **2019**, *60*, No. E50−E57.

(11) Portes, D. B.; Abeldt, L. W.; dos Santos Giuberti, C.; Endringer, D. C.; Pimentel, E. F. Development of natural cosmetic emulsion using the by-product of *Lecythis pisonis* seed. *Toxicol. In Vitro* **2024**, *97*, 105791.

(12) Adnan, M.; Siddiqui, A. J.; Ashraf, S. A.; Snoussi, M.; Badraoui, R.; Alreshidi, M.; Elasbali, A. M.; Al-Soud, W. A.; Alharethi, S. H.; Sachidanandan, M.; Patel, M. Polyhydroxybutyrate (PHB)-based biodegradable polymer from *Agromyces indicus*: Enhanced production, characterization, and optimization. *Polymers* **2022**, *14*, 3982.

(13) Orhan, F.; Akıncıoğlu, A.; Ceyran, E. Ectoine production from a novel bacterial strain and high-purity purification with a cost-effective and single-step method. *J. Biotechnol.* **2024**, *388*, 24.

(14) Soberón-Chávez, G.; González-Valdez, A.; Soto-Aceves, M. P.; Cocotl-Yañez, M. Rhamnolipids produced by Pseudomonas: From molecular genetics to the market. *Microb. Biotechnol.* **2021**, *14*, 136.

(15) Vicente, D.; Proença, D. N.; Morais, P. V. The Role of Bacterial Polyhydroalkanoate (PHA) in a Sustainable Future: A Review on the Biological Diversity. *Int. J. Environ. Res. Public Health* **2023**, *20*, 2959.
(16) Dalsasso, R. R.; Pavan, F. A.; Bordignon, S. E.; de Aragão, G. M. F.; Poletto, P. Polyhydroxybutyrate (PHB) production by *Cupriavidus necator* from sugarcane vinasse and molasses as mixed substrate. *Process Biochem.* **2019**, *85*, 12−18.
(17) Zhang, L.; Jiang, Z.; Tsui, T.-H.; Loh, K. C.; Dai, Y.; Tong, Y. W. A Review on enhancing *Cupriavidus necator* fermentation for poly(3-hydroxybutyrate) (PHB) production from low-cost carbon sources. *Front. Bioeng. Biotechnol.* **2022**, *10*, 946085.
(18) Suehs, B. A.; Yamamoto, F. Y.; Asiri, F.; Gatlin, D. M. Poly-*β*-hydroxybutyrate has limited effects on growth and immune responses of juvenile hybrid striped bass Morone chrysops × M. saxatilis, and red drum Sciaenops ocellatus based on in vivo and in vitro approaches. *Aquaculture* **2023**, *570*, 739429.
(19) Amir, M.; Rizvi, S. F.; Asif, M.; Ahmad, A.; Alshammari, M. B.; Gupta, A.; Zaheer, M. H.; Roohi, R. Polyhydroxybutyrate (PHB) bioplastic characterization from the isolate Pseudomonas stutzeri PSB1 synthesized using potato peel feedstock to combat solid waste management. *Biocatal. Agric. Biotechnol.* **2024**, *57*, 103097.
(20) Kang, J.; Yun, S. I. Chitosan-reinforced PHB hydrogel and aerogel monoliths fabricated by phase separation with the solvent-exchange method. *Carbohydr. Polym.* **2022**, *284*, 119184.
(21) Phothong, N.; Boontip, T.; Chouwatat, P.; Aht-Ong, D.; Napathorn, S. C. Preparation and characterization of astaxanthin-loaded biodegradable polyhydroxybutyrate (PHB) microbeads for personal care and cosmetic applications. *Int. J. Biol. Macromol.* **2024**, *257*, 128709.
(22) Engler, L. G.; Farias, N. C.; Crespo, S. J.; Gately, N. M.; Major, I.; Pezzoli, R.; Devine, D. M. Designing sustainable polymer blends: Tailoring mechanical properties and degradation behaviour in PHB/PLA/PCL blends in a seawater environment. *Polymers* **2023**, *15*, 2874.
(23) Lin, X.; Fan, X.; Li, R.; Li, Z.; Ren, T.; Ren, X.; Huang, T.-S. Preparation and characterization of PHB/PBAT−based biodegradable antibacterial hydrophobic nanofibrous membranes. *Polym. Adv. Technol.* **2018**, *29*, 481−489.
(24) Coltelli, M.-B.; Panariello, L.; Morganti, P.; Danti, S.; Baroni, A.; Lazzeri, A.; Fusco, A.; Donnarumma, G. Skin-compatible biobased beauty masks prepared by extrusion. *J. Funct. Biomater.* **2020**, *11*, 23.
(25) Bokrova, J.; Marova, I.; Matouskova, P.; Pavelkova, R. Fabrication of novel PHB-liposome nanoparticles and study of their toxicity in vitro. *J. Nanopart. Res.* **2019**, *21*, 49.
(26) Voinova, V. V.; Zhuikov, V. A.; Zhuikova, Y. V.; Sorokina, A. A.; Makhina, T. K.; Bonartseva, G. A.; Parshina, E. Y.; Hossain, M. A.; Shaitan, K. V.; Pryadko, A. S.; et al. Adhesion of *Escherichia coli* and *Lactobacillus fermentum* to films and electrospun fibrous scaffolds from composites of poly(3-hydroxybutyrate) with magnetic nanoparticles in a low-frequency magnetic field. *Int. J. Mol. Sci.* **2023**, *25*, 208.
(27) Gazvoda, L.; Perišić, N. M.; Spreitzer, M.; Vukomanović, M. Antimicrobial activity of piezoelectric polymer: Piezoelectricity as the reason for damaging bacterial membrane. *Biomater. Sci.* **2022**, *10*, 4933−4948.
(28) Choi, Y.; Choi, K. Y. Indirubin-incorporated biodegradable PHB microbeads and its application for functional facial cleanser. *Dyes Pigm.* **2025**, *235*, 112586.
(29) Li, X.; Wei, J.; Lin, L.; Zheng, G. Extraction, moisturizing activity and potential application in skin cream of Akebia trifoliata (Thunb.) Koidz polysaccharide. *Ind. Crops Prod.* **2023**, *197*, 116613.
(30) Czech, L.; Hermann, L.; Stöveken, N.; Richter, A.; Höppner, A.; Smits, S.; Heider, J.; Bremer, E. Role of the extremolytes ectoine and hydroxyectoine as stress protectants and nutrients: Genetics, phylogenomics, biochemistry, and structural analysis. *Genes* **2018**, *9*, 177.
(31) Cantera, S.; Tamarit, D.; Strong, P. J.; Sánchez-Andrea, I.; Ettema, T. J. G.; Sousa, D. Z. Prospective CO_2 and CO bioconversion into ectoines using novel microbial platforms. *Rev. Environ. Sci. Bio/technol.* **2022**, *21*, 571−581.
(32) Graf, R.; Anzali, S.; Buenger, J.; Pfluecker, F.; Driller, H. The multifunctional role of ectoine as a natural cell protectant. *Clin. Dermatol.* **2008**, *26*, 326−333.
(33) Marini, A.; Reinelt, K.; Krutmann, J.; Bilstein, A. Ectoine-containing cream in the treatment of mild to moderate atopic dermatitis: A randomised, comparator-controlled, intra-individual double-blind, multi-center trial. *Skin Pharmacol. Physiol.* **2014**, *27*, 57−65.
(34) Alexander, S.; Barron, A. R.; Denkov, N.; Grassia, P.; Kiani, S.; Sagisaka, M.; Shojaei, M. J.; Shokri, N. Foam generation and stability: Role of the surfactant structure and asphaltene aggregates. *Ind. Eng. Chem. Res.* **2022**, *61*, 372−381.
(35) McClements, D. J.; Jafari, S. M. Improving emulsion formation, stability and performance using mixed emulsifiers: A review. *Adv. Colloid Interface Sci.* **2018**, *251*, 55−79.
(36) Zhu, F.; Cao, C.; Cao, L.; Li, F.; Du, F.; Huang, Q. Wetting behavior and maximum retention of aqueous surfactant solutions on tea leaves. *Molecules* **2019**, *24*, 2094.
(37) Badmus, S. O.; Amusa, H. K.; Oyehan, T. A.; Saleh, T. A. Environmental risks and toxicity of surfactants: Overview of analysis, assessment, and remediation techniques. *Environ. Sci. Pollut. Res.* **2021**, *28*, 62085.
(38) Jurek, I.; Szuplewska, A.; Chudy, M.; Wojciechowski, K. Soapwort (Saponaria officinalis L.) extract vs. synthetic surfactants effect on skin-mimetic models. *Molecules* **2021**, *26*, 5628.
(39) Martins, M. S.; Ferreira, M. S.; Almeida, I. F.; Sousa, E. Occurrence of allergens in cosmetics for sensitive skin. *Cosmetics* **2022**, *9*, 32.
(40) Moldes, A. B.; Rodríguez-López, L.; Rincón-Fontán, M.; López-Prieto, A.; Vecino, X.; Cruz, J. M. Synthetic and bio-derived surfactants versus microbial biosurfactants in the cosmetic industry: An overview. *Int. J. Mol. Sci.* **2021**, *22*, 2371.
(41) Eslami, P.; Hajfarajollah, H.; Bazsefidpar, S. Recent advancements in the production of rhamnolipid biosurfactants by Pseudomonas aeruginosa. *RSC Adv.* **2020**, *10*, 34014.
(42) Abdel-Mawgoud, A. M.; Lépine, F.; Déziel, E. Rhamnolipids: Diversity of structures, microbial origins and roles. *Appl. Microbiol. Biotechnol.* **2010**, *86*, 1323−1336.
(43) dos Santos, S. C.; Torquato, C. A.; de Alexandria Santos, D.; Orsato, A.; Leite, K.; Serpeloni, J. M.; Losi-Guembarovski, R.; Pereira, E. R.; Dyna, A. L.; Barboza, M. G. L.; et al. Production and characterization of rhamnolipids by Pseudomonas aeruginosa isolated in the Amazon region, and potential antiviral, antitumor, and antimicrobial activity. *Sci. Rep.* **2024**, *14*, 4629.
(44) Hahn, T.; Alzate, M. O.; Leonhardt, S.; Tamang, P.; Zibek, S. Current trends in medium-chain-length polyhydroxyalkanoates: Microbial production, purification, and characterization. *Eng. Life Sci.* **2024**, *24*, 2300211.
(45) Wu, J.; Ju, L. K. Extracellular particles of polymeric material formed in n-hexadecane fermentation by *Pseudomonas aeruginosa*. *J. Biotechnol.* **1998**, *59*, 193−202.
(46) Hogan, D. E.; Curry, J. E.; Pemberton, J. E.; Maier, R. M. Rhamnolipid biosurfactant complexation of rare earth elements. *J. Hazard. Mater.* **2017**, *340*, 171−178.
(47) Adu, S. A.; Twigg, M. S.; Naughton, P. J.; Marchant, R.; Banat, I. M. Biosurfactants as anticancer agents: Glycolipids affect skin cells in a differential manner dependent on chemical structure. *Pharmaceutics* **2022**, *14*, 360.
(48) Buonocore, C.; Giugliano, R.; Sala, G. D.; Esposito, F. P.; Tedesco, P.; Folliero, V.; Galdiero, M.; Franci, G.; de Pascale, D. Evaluation of antimicrobial properties and potential applications of pseudomonas gessardii m15 rhamnolipids towards multiresistant *Staphylococcus aureus*. *Pharmaceutics* **2023**, *15*, 700.
(49) Adu, S. A.; Twigg, M. S.; Naughton, P. J.; Marchant, R.; Banat, I. M. Glycolipid biosurfactants in skincare applications: Challenges and recommendations for future exploitation. *Molecules* **2023**, *28*, 4463.
(50) Raszewska-Famielec, M.; Flieger, J. Nanoparticles for topical application in the treatment of skin dysfunctions−an overview of

https://doi.org/10.1021/acsomega.4c10583
ACS Omega 2025, 10, 12200−12213

dermo-cosmetic and dermatological products. *Int. J. Mol. Sci.* **2022**, *23*, 15980.
(51) Lenz, R. W.; Marchessault, R. H. Bacterial polyesters: Biosynthesis, biodegradable plastics and biotechnology. *Biomacromolecules* **2005**, *6*, 1−8.
(52) Hazer, B.; Steinbüchel, A. Increased diversification of polyhydroxyalkanoates by modification reactions for industrial and medical applications. *Appl. Microbiol. Biotechnol.* **2007**, *74*, 1−12.
(53) Hazer, D. B.; Kılıçay, E.; Hazer, B. Poly(3-hydroxyalkanoate)s: Diversification and biomedical applications. *Mater. Sci. Eng.* **2012**, *32*, 637−647.
(54) El-Malek, F. A.; Steinbüchel, A. Post-synthetic enzymatic and chemical modifications for novel sustainable polyesters. *Front. Bioeng. Biotechnol.* **2022**, *9*, 817023.
(55) Domenek, S.; Langlois, V.; Renard, E. Bacterial polyesters grafted with poly(ethylene glycol): Behaviour in aqueous media. *Polym. Degrad. Stab.* **2007**, *92*, 1384−1392.
(56) Hazer, B.; Eren, M.; Senemoğlu, Y.; Modjinou, T.; Renard, E.; Langlois, V. Novel poly(3-hydroxy butyrate) macro RAFT agent: Synthesis and characterization of thermoresponsive block copolymers. *J. Polym. Res.* **2020**, *27*, 147.
(57) Koçer, H.; Borcakli, M.; Demirel, S.; Hazer, B. Production of bacterial polyesters from some various new substrates by *Alcaligenes eutrophus* and *Pseudomonas oleovorans*. *Turk. J. Chem.* **2003**, *27*, 365−373.
(58) Chen, G. Q. A microbial polyhydroxyalkanoates (PHA) based bio- and materials industry. *Chem. Soc. Rev.* **2009**, *38*, 2434.
(59) Ashby, R. D.; Foglia, T. A. Poly(hydroxyalkanoate) biosynthesis from triglyceride substrates. *Appl. Microbiol. Biotechnol.* **1998**, *49*, 431−437.
(60) Wickramathilaka, M. P.; Tao, B. Y. Characterization of covalent crosslinking strategies for synthesizing DNA-based bioconjugates. *J. Biol. Eng.* **2019**, *13*, 63.
(61) Rivera-Santiago, R. F.; Sriswasdi, S.; Harper, S. L.; Speicher, D. W. Probing structures of large protein complexes using zero-length cross-linking. *Methods* **2015**, *89*, 99−111.
(62) Ghosh, A. K.; Shahabi, D. Synthesis of amide derivatives for electron deficient amines and functionalized carboxylic acids using EDC and DMAP and a catalytic amount of HOBt as the coupling reagents. *Tetrahedron Lett.* **2021**, *63*, 152719.
(63) Sionkowska, A.; Kulka-Kamińska, K.; Brudzyńska, P.; Lewandowska, K.; Piwowarski, Ł. The influence of various cross-linking conditions of EDC/NHS on the properties of fish collagen film. *Mar. Drugs* **2024**, *22*, 194.
(64) Tanne, C.; Golovina, E. A.; Hoekstra, F. A.; Meffert, A.; Galinski, E. A. Glass-forming property of hydroxyectoine is the cause of its superior function as a desiccation protectant. *Front. Microbiol.* **2014**, *5*, 00150.
(65) Rizki, W. O. S.; Ratnaningsih, E.; Hertadi, R. Production of poly-(R)-3-hydroxybutyrate from halophilic bacterium Salinivibrio sp. utilizing palm oil mill effluent as a carbon source. *Biocatal. Agric. Biotechnol.* **2023**, *47*, 102558.
(66) Ji, Y.; Yang, X.; Ji, Z.; Zhu, L.; Ma, N.; Chen, D.; Jia, X.; Tang, J.; Cao, Y. DFT-calculated IR spectrum amide I, II, and III band contributions of N-methylacetamide fine components. *ACS Omega* **2020**, *5*, 8572.
(67) Dmour, I.; Taha, M. O. Natural and semisynthetic polymers in pharmaceutical nanotechnology. In *Organic Materials as Smart Nanocarriers for Drug Delivery*, Grumezescu, A. M., Ed.; Elsevier Inc: Amsterdam, 2018, pp. 35−100.
(68) Lathwal, P.; Nehra, K.; Singh, M.; Rana, J. S. Characterization of novel and efficient poly-3-hydroxybutyrate (PHB) producing bacteria isolated from Rhizospheric Soils. *J. Polym. Environ.* **2018**, *26*, 3437−3450.
(69) Anburajan, L.; Meena, B.; Sreelatha, T.; Vinithkumar, N. V.; Kirubagaran, R.; Dharani, G. Ectoine biosynthesis genes from the deep sea halophilic eubacteria, *Bacillus clausii* NIOT-DSB04: Its molecular and biochemical characterization. *Microb. Pathog.* **2019**, *136*, 103693.
(70) Trakunjae, C.; Boondaeng, A.; Apiwatanapiwat, W.; Kosugi, A.; Arai, T.; Sudesh, K.; Vaithanomsat, P. Enhanced polyhydroxybutyrate (PHB) production by newly isolated rare actinomycetes Rhodococcus sp. strain BSRT1-1 using response surface methodology. *Sci. Rep.* **2021**, *11*, 1896.
(71) Moura, C. C.; Salazar-Bryam, A. M.; Piazza, R. D.; Carvalho dos Santos, C.; Jafelicci, M.; Marques, R. F. C.; Contiero, J. Rhamnolipids as green stabilizers of nZVI and application in the removal of nitrate from simulated groundwater. *Front. Bioeng. Biotechnol.* **2022**, *10*, 794460.
(72) Li, R.; Jiang, Y.; Wang, X.; Yang, J.; Gao, Y.; Zi, X.; Zhang, X.; Gao, H.; Hu, N. Psychrotrophic Pseudomonas mandelii CBS-1 produces high levels of poly-β-hydroxybutyrate. *Springerplus* **2013**, *2*, 335.
(73) Van Thuoc, D.; Loan, T. T.; Tra, N. T. Accumulation of ectoines by *Halophilic Bacteria* isolated from fermented shrimp paste: An adaptation mechanism to salinity, temperature, and pH stress. *Curr. Microbiol.* **2021**, *78*, 2355−2366.
(74) Sabarinathan, D.; Chandrika, S. P.; Venkatraman, P.; Easwaran, M.; Sureka, C. S.; Preethi, K. Production of polyhydroxybutyrate (PHB) from *Pseudomonas plecoglossicida* and its application towards cancer detection. *Inform. Med. Unlocked* **2018**, *11*, 61−67.
(75) Balakrishna, P. A.; Kumar, A. J.; Thulasi, K.; Kumarapillai, H. Evaluation of short-chain-length polyhydroxyalkanoate accumulation in *Bacillus aryabhattai*. *Braz. J. Microbiol.* **2017**, *48*, 451−460.
(76) Chen, J.; Liu, P.; Chu, X.; Chen, J.; Zhang, H.; Rowley, D. C.; Wang, H. Metabolic pathway construction and optimization of *Escherichia coli* for high-level ectoine production. *Curr. Microbiol.* **2020**, *77*, 1412−1418.
(77) Babij, N. R.; McCusker, E. O.; Whiteker, G. T.; Canturk, B.; Choy, N.; Creemer, L. C.; De Amicis, C. V.; Hewlett, N. M.; Johnson, P. L.; Knobelsdorf, J. A.; et al. NMR chemical shifts of trace impurities: Industrially preferred solvents used in process and green chemistry. *Org. Process Res. Dev.* **2016**, *20*, 661−667.
(78) Mezzi, A.; Caro, T.; Riccucci, C.; Faraldi, F.; Veroli, C.; Caschera, D. Unusual surface degradation products grown on archaeological bronze artefacts. *Appl. Phys. A.* **2013**, *113*, 1121−1128.
(79) Corrado, I.; Di Girolamo, R.; Regalado-González, C.; Pezzella, C. Polyhydroxyalkanoates-based nanoparticles as essential oil carriers. *Polymers* **2022**, *14*, 166.
(80) Aguilar-Rabiela, A. E.; Hernández-Cooper, E. M.; Otero, J. A.; Vergara-Porras, B. Modeling the release of curcumin from microparticles of poly(hydroxybutyrate) [PHB]. *Int. J. Biol. Macromol.* **2020**, *144*, 47−52.
(81) Duffy, J. J.; Panalytical, M.; Hill, A. J. Suspension Stability; Why Particle Size, Zeta Potential and Rheology Are Important. *Annu. Trans. -Nord. Rheol. Soc.* **2012**, *20*, 209−214.
(82) Helmy, Q.; Gustiani, S.; Mustikawati, A. Application of rhamnolipid biosurfactant for bio-detergent formulation. *IOP Conf Ser. Mater. Sci. Eng.* **2020**, *823*, 012014.
(83) Wojciechowski, K.; Klodzinska, E. Zeta potential study of biodegradable antimicrobial polymers. *Colloids Surf., A* **2015**, *483*, 204−208.
(84) Wu, Y. C.; Wei, Y. H.; Wu, H. S. Adsorption and desorption behavior of ectoine using Dowex® HCR-S Ion-Exchange Resin. *Processes* **2021**, *9*, 2068.
(85) Murdoc, R. C.; Braydich-Stoll, L.; Schrand, A. M.; Schlager, J. J.; Hussain, S. M. Characterization of nanomaterial dispersion in solution prior to in vitro exposure using dynamic light scattering technique. *Toxicol. Sci.* **2008**, *101*, 239−253.
(86) Darie-Ion, L.; Jayathirtha, M.; Hitruc, G. E.; Zaharia, M. M.; Gradinaru, R. V.; Darie, C. C.; Pui, A.; Petre, B. A. A proteomic approach to identify zein proteins upon eco-friendly ultrasound-based extraction. *Biomolecules* **2021**, *11*, 1838.
(87) Tinoco, A.; Gonçalves, F.; Costa, A. F.; Freitas, D. S.; Cavaco-Paulo, A.; Ribeiro, A. K. Keratin: Zein particles as vehicles for fragrance release on hair. *Ind. Crops Prod.* **2021**, *159*, 113067.
(88) Gidudu, B.; Chirwa, E. M. N. Evaluation of the toxicity of a rhamnolipid biosurfactant for its application in the optimization of the

https://doi.org/10.1021/acsomega.4c10583
ACS Omega 2025, 10, 12200−12213

bio-electrokinetic remediation of petrochemical contaminated soil. *Clean. Eng. Technol.* **2022**, *9*, 100521.
(89) Bujak, T.; Zagórska-Dziok, M.; Nizioł-Łukaszewska, Z. Complexes of ectoine with the anionic surfactants as active ingredients of cleansing cosmetics with reduced irritating potential. *Molecules* **2020**, *25*, 1433.
(90) Shanbhag, S.; Nayak, A.; Narayan, R.; Nayak, U. Y. Anti-aging and sunscreens: Paradigm shift in cosmetics. *Adv. Pharm. Bull.* **2019**, *9*, 348−359.
(91) Sahariah, B. K.; Sarma. Spectroscopic evidence of n → π^* interactions involving carbonyl groups. *Phys. Chem. Chem. Phys.* **2020**, *22*, 26669−26681.
(92) Jiang, S. J.; Chu, A. W.; Lu, Z. F.; Pan, M. H.; Che, D. F.; Zhou, X. J. Ultraviolet B-induced alterations of the skin barrier and epidermal calcium gradient. *Exp. Dermatol.* **2007**, *16*, 985.
(93) Takagi, Y.; Nakagawa, H.; Kondo, H.; Takema, Y.; Imokawa, G. Decreased levels of covalently bound ceramide are associated with ultraviolet B-induced perturbation of the skin barrier. *J. Invest. Dermatol.* **2004**, *123*, 1102−1109.
(94) Biniek, K.; Levi, K.; Dauskardt, R. H. Solar UV radiation reduces the barrier function of human skin. *Proc. Natl. Acad. Sci. U. S. A.* **2012**, *109*, 17111−17116.
(95) Frickmann, H.; Hahn, A.; Berlec, S.; Ulrich, J.; Jansson, M.; Schwarz, N. G.; Warnke, P.; Podbielski, A. On the etiological relevance of *Escherichia coli* and *Staphylococcus aureus* in superficial and deep infections − a hypothesis-forming, retrospective assessment. *Eur. J. Microbiol. Immunol.* **2019**, *9*, 124−130.
(96) Alyousif, N. A.; Al-Tamimi, W.; YAl-luaibi, Y. Y. Y. Antimicrobial and antioxidant activity of rhamnolipids biosurfactant is produced by Pseudomonas aeruginosa. *Rev. Bionatura* **2023**, *8*, 1−11.
(97) de Freitas Ferreira, J.; Vieira, E. A.; Nitschke, M. The antibacterial activity of rhamnolipid biosurfactant is pH dependent. *Food Res. Int.* **2019**, *116*, 737−744.
(98) Gajic, I.; Kabic, J.; Kekic, D.; Jovicevic, M.; Milenkovic, M.; Culafic, D. M.; Trudic, A.; Ranin, L.; Opavski, N. Antimicrobial susceptibility testing: A comprehensive review of currently used methods. *Antibiotics* **2022**, *11*, 427.
(99) Cavassin, E. D.; de Figueiredo, L. F. P.; Otoch, J. P.; Seckler, M. M.; de Oliveira, R. A.; Franco, F. F.; Marangoni, V. S.; Zucolotto, V.; Levin, A. S. S.; Costa, S. F. Comparison of methods to detect the in vitro activity of silver nanoparticles (AgNP) against multidrug resistant bacteria. *J. Nanobiotechnol.* **2015**, *13*, 64.
(100) Otto, M. *Staphylococcus* colonization of the skin and antimicrobial peptides. *Expert Rev. Dermatol.* **2010**, *5*, 183−195.
(101) Thakur, P.; Saini, N. K.; Thakur, V. K.; Gupta, V. K.; Saini, R. V.; Saini, A. K. Rhamnolipid the glycolipid biosurfactant: Emerging trends and promising strategies in the field of biotechnology and biomedicine. *Microb. Cell Fact.* **2021**, *20*, 1.
(102) Prajapati, A.; Srivastava, A. Preparation, characterization and encapsulation efficiency of egg albumin nanoparticles using EDC as crosslinker. *J. Sci. Ind. Res.* **2019**, *78*, 703−705.
(103) Gars, M. L.; Roger, P.; Belgacem, N.; Bras, J. Role of solvent exchange in dispersion of cellulose nanocrystals and their esterification using fatty acids as solvents. *Cellulose* **2020**, *27*, 4319−4336.
(104) Boroujeni, M. B.; Nayeri, H. Stabilization of bovine lactoperoxidase in the presence of ectoine. *Food Chem.* **2018**, *265*, 208−215.
(105) Anburajan, L.; Meena, B.; Sreelatha, T.; Vinithkumar, N. V.; Kirubagaran, R.; Dharani, G. Ectoine biosynthesis genes from the deep-sea halophilic eubacteria, *Bacillus clausii* NIOT-DSB04: Its molecular and biochemical characterization. *Microb. Pathog.* **2019**, *136*, 103693.
(106) Vahabi, H.; Michely, L.; Moradkhani, G.; Akbari, V.; Cochez, M.; Vagner, C.; Renard, E.; Saeb, M. R.; Langlois, V. Thermal stability and flammability behavior of poly(3-hydroxybutyrate) (PHB) based composites. *Materials* **2019**, *12*, 2239.
(107) Tian, J.; He, A.; Lawrence, A. G.; Liu, P.; Watson, N.; Sinskey, A. J.; Stubbe, J. Analysis of transient polyhydroxybutyrate production in Wautersia eutropha H16 by quantitative western analysis and Transmission Electron Microscopy. *J. Bacteriol.* **2005**, *187*, 3825.
(108) Radakisnin, R.; Majid, M. S. A.; Jamir, M. R. M.; Jawaid, M.; Sultan, M. T. H.; Tahir, M. F. M. Structural, morphological and thermal properties of cellulose nanofibers from napier fiber (Pennisetum purpureum). *Materials* **2020**, *13*, 4125.
(109) Cohen, L.; Sanchez, E.; Martin, M.; Soto, F.; Trujillo, F. Study of the effects of LAS and zein concentrations on protein solubilization. *J. Surfactants Deterg.* **2016**, *19*, 1089−1092.
(110) Pavelkova, R.; Matouskova, P.; Hoova, J.; Porizka, J.; Marova, I. Preparation and characterization of organic UV filters based on combined PHB/liposomes with natural phenolic compounds. *J. Biotechnol.* **2020**, *324*, 100021.
(111) Balouiri, M.; Sadiki, M.; Ibnsouda, S. K. Methods for in vitro evaluating antimicrobial activity: A review. *J. Pharm. Anal.* **2016**, *6*, 71−79.

https://doi.org/10.1021/acsomega.4c10583
ACS Omega 2025, 10, 12200−12213